# A Low-Profile Dual-Polarized Antenna with High Isolation and High Front-to-Back Ratio for 5G Base Stations

**M. Ciydem**

Department of Electrical and Electronics Engineering
Faculty of Engineering, Gazi University, Ankara, 06570, Turkey
mehmetciydem@gazi.edu.tr

***Abstract*** ─ A dual-polarized, broadband, slot-coupled patch antenna design is presented for sub-6 GHz 5G base stations. Proposed antenna is made up of two suspended stacked patches above feedline layer and is excited by crossed elliptic-H slots for ±45º slant, linear dual polarized operation. Prototyped antenna has an impedance bandwidth of 22.1% (3.14 - 3.92 GHz) for $|S_{11}|$, $|S_{22}|$ < −15 dB and port isolation $|S_{21}|$ is also obtained to be < −28 dB in this band. Antenna exhibits directional radiation patterns with half power beamwidths of 57º - 65º and 60º - 64º in elevation and azimuth planes, respectively with varying gain of 8.6 - 9.1 dBi. Proposed antenna is also low profile (11.1 mm) with high front-to-back ratio (> 27 dB) without reflector. Design details, numerical studies, and measurement results are presented.

***Index Terms*** ─ Dual-polarized, broadband antenna, isolation, front-to-back ratio, sub-6 GHz 5G base stations.

## I. INTRODUCTION

Continuous increasing demands in data rates, bandwidth (BW) and quality of services (QoS) in cellular communication put challenging requirements for base station antennas such as being dual-polarization, low profile, broadband impedance matching ($|S_{11}|$, $|S_{22}|$ < −15 dB), high port isolation ($|S_{21}|$ < −20 dB), and high front-to-back ratio (FBR > 20 dB). 5G is a promising technology with massive multiple input multiple output (mMIMO) antenna arrays, which is one of the key enabling technologies of 5G, to meet the demands of celullar industry. N78 band (3.30-3.80 GHz) is assigned for sub-6 GHz 5G applications. Making full use of mMIMO requires further performance improvements such as isolation $|S_{21}|$ < −25 dB and FBR > 25 dB. Design of single element antenna with high isolation and high front-to-back ratio helps mMIMO array to reach these performance levels easily. Moreover mMIMO arrays are bulky structures with huge number of antenna elements. Outdoor physical installation requirements necessitates mMIMO array to be compact and low profile. Therefore it is still a challenging problem to design dual-polarized, broadband antenna element with high isolation, high FBR and low profile in a simple configuration.

Patch antennas are widely used in dual-polarized base station antennas because of their compactness, low profile, and ease of manufacturing [1]. Despite their narrowband nature at the beginning, different feeding techniques have been developed to make them broadband. Probe feeding and slot coupling are common methods for exciting the patches. Together with such feeding mechanism, stacked patch antennas (SPAs) can also be employed for broadband operation. Several variations of probe feeding (L, T, F, meandering, and hook shapes, symmetric or anti-symmetric feeds) for dual-polarized patch antennas are introduced in [2-8]. Other common type of feeding is slot coupling in single or multilayer configurations. Dual-polarization feature of patch is accomplished by either crossed slots centered on common ground or two separate slots in orthogonal placement [9-14]. Crossed-slot geometry is more common because of its single layer feeding, making the antenna low profile and compact. In [9], a dual-polarized SPA is designed by utilizing a plus-like shaped slot. A four layer microstrip patch antenna is presented in [10] where the feeding lines for each polarization are mounted on separate layers and slots are etched on these layers accordingly. In [11], two modified-H slots are used to create dual-polarization on the patch. [12-13] reports square shaped ring slot structure feeding a patch and Jerusalem crossed radiator, respectively. In [14], a broadband multilayer SPA containing a quasi-crossed-shaped slot is presented. Furher different designs of slot coupled antennas can be found in [15-16].

Slot-coupled patch antennas may be simple, low profile however their FBR performance is poor because of undesirable back radiation of the slots. Hence additional reflector plane or cavity backed structure, which increases antenna profile, is generally employed to make FBR higher. Isolation between ports is also another problem in SPA design due to the mutual coupling of currents flowing in the slot plane. Additional reflector plane to improve the FBR may form a waveguide

*Submitted On: April 17, 2021*
*Accepted On: July 6, 2021*
https://doi.org/10.47037/2021.ACES.J.360916

with the ground plane causing flow of unwanted higher order currents and poor isolation. In order to improve the isolation, electromagnetic band-gap (EBG) and meta-material based superstrates have been proposed [17, 18].

In this paper, design of a simple, dual-polarized, slot-coupled SPA with easy fabrication is presented for sub-6 GHz 5G base stations to operate in 3.30-3.80 GHz band. Different than other works, elliptic-H slots are employed for exciting the patches. Design of stacked patches (dimensions and placement) are made in such way that that proposed SPA exhibits 22.1% (3.14-3.92 GHz) impedance BW for $|S_{11}|$, $|S_{22}| < -15$ dB, with a gain of 8.6-9.1 dBi. Broadside, directional radiation patterns have been obtained with half power beamwidths (HPBWs) of 57°- 65° and 60°- 64° in elevation and azimuth planes, respectively. Moreover, in addition to these performances, other prominent features of the proposed antenna can be counted as its high FBR (> 27 dB) and high isolation ($|S_{21}| < -28$) with low profile (11.1 mm). And they have been achieved without use of any additional reflector, cavity backed structure and EBG or meta-material based surface in the design.

This paper is organized as follows. Section II describes geometry, configuration and physical dimensions of proposed SPA with working principles. Section III deals with numerical studies including parametric studies and performance optimizations. Section IV presents measurement results while Section V discusses the study and concludes the work with detailed comparison of previous related ones showing the superior performance of proposed antenna.

## II. ANTENNA DESIGN

### A. Geometry and configuration

Geometry and configuration of SPA is illustrated in Fig. 1 while its physical dimensions are given in Table 1. SPA comprises two suspended stacked patches (main one and parasitic one) and a feedline layer, all separated by air. Heights of the main and parasitic patches are denoted by $h_{s1}$ and $h_{s2}$, respectively. Patches are 0.25 mm thick metal squares whose sides are $L_{s1}$ and $L_{s2}$. The feedline layer consists of a feed network at its bottom side and a common ground at its upper side. Elliptic-H slots are etched on this ground side. Feed network is composed of two parts: matching section and 100 Ω branch lines. Matching section provides broadband matching between input impedance of SPA and 50 Ω SMA port. It includes a two-section binomial transformer and an additional rectangular stub of size 3.1 × 4.0 mm$^2$. Transformer sections are approximately quarter wavelength ($L_{t1}$, $L_{t2}$) at the center frequency, $f_c$ = 3.55 GHz ($\lambda_c$ = 84.5 mm). Coupling to the slots is realized by two 100 Ω microstrip branch lines which are connected to the matching section by a T-junction. Branch lines are separated by a distance $L_d$ and terminated by L-shaped stubs in order to compensate the reactive component of the input impedance of SPA and preclude the overlap. Line crossing between inner branches is inevitable and hence a small air bridge is introduced here to avoid intersection. Feedline layer is implemented on FR4 substrate ($\varepsilon_r$ = 4.4, tan$\delta$ = 0.02) of 1.6 mm thickness.

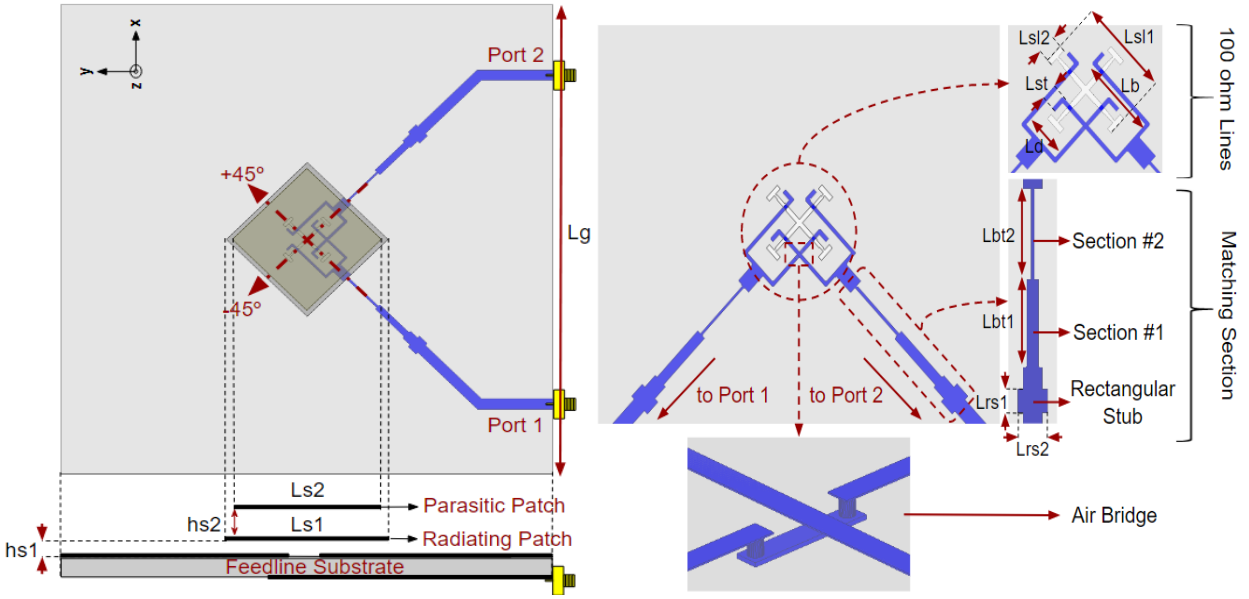


Fig. 1. Antenna geometry and configuration (a) top view and cross-section, and (b) elliptic-H slots, feedlines and binomial transformer.

Table 1: Physical dimensions of the proposed antenna

| Description | Parameter | Dimensions (mm) |
|---|---|---|
| Ground plane | $L_g$ | 110 |
| Main patch | $L_{s1}$ | 32.5 |
| Parasitic patch | $L_{s2}$ | 30 |
| Lower/Upper air height | $h_{s1}$, $h_{s2}$ | 2, 7 |
| Slot major axis length | $L_{sl1}$ | 16.5 |
| Vertical slot width | $L_{sl2}$ | 3.2 |
| Stub Length | $L_{st}$ | 2.35 |
| 1st binomial section length | $L_{bt1}$ | 11.55 |
| 2nd binomial section length | $L_{bt2}$ | 11.82 |
| Branch lines separation | $L_d$ | 6.91 |
| Rectangular stub length/width | $L_{rs1}$, $L_{rs2}$ | 3.1, 4 |
| FR4 height | $h$ | 1.6 |
| Overall SPA height | 2+7+1.6+2x0.25 = 11.1 | |

### B. Working principles

Electromagnetic power is coupled to patches through elliptic-H slots and ±45° dual polarizations are created. Dimensions and placement of patches at proper heights are of critical importance for good broadband matching, isolation and FBR. Although main patch ($L_{s1}$, $h_{s1}$) has dominant effect in total design, parasitic one ($L_{s2}$, $h_{s2}$) must also be considered in combination with it to reach desired performance. The lower $h_{s1}$ makes efficient coupling from slots to SPA easier, hence resulting in good FBR. However, this lower $h_{s1}$ makes broadband operation difficult. The higher $h_{s1}$ facilitates broadband operation but efficient coupling from slots to SPA becomes more difficult and hence resulting in poor FBR. The existence of parasitic patch may be questioned because it increases the overall antenna profile. However, as shown in the next section, desired technical performances cannot be obtained by a single patch and hence parasitic one is also required. The basic idea of the design is to place main patch at the lowest possible height ($h_{s1}$) to have good FBR, and at the same with the proper combination of both patches ($h_{s1}$, $h_{s2}$), to reach desired impedance BW, matching level, isolation, and to keep overall SPA still profile low. Proper placement of the second patch (parasitic patch) with the main patch modifies the current distribution on the main patch. And vectorial combination of currents flowing on the two patches has a total effect of improving the isolation.

In this work, different than conventional rectangular-H slots, central sections of the slots are designed in elliptic form. As addressed in [19], elliptic slot is a simple technique for broadband efficient coupling between microstrip transitions and employed here as coupled-feeding mechanism. Axial ratio ($A_x$) of the ellipse, specifically length of its major axis, controls the level of the coupling. Tapered line nature of slots due to elliptic shape provides further separation between slots around the center where most coupling occurs and improves the isolation. Furthermore, elliptic shape of slots also provides better impedance matching and efficient power transfer from slots to the patches. This yields less return power and less flowing currents in the slot plane resulting in less backward radiation (high FBR) and less mutual coupling currents (high isolation).

Figure 2 plots surface current distributions on the main and parasitic patches at 3.30 GHz and 3.80 GHz when SPA is excited at port 1. Current amplitude on the main patch gradually increases towards edges at 3.30 GHz in symmetry with +45º diagonal line while the currents are weaker on the parasitic one. At 3.80 GHz, stronger coupling occurs between two patches and current amplitude on the parasitic patch increases while it remains almost same with little decrease on the main patch. This means that resonant behaviour around 3.80 GHz is mostly governed by the parasitic patch.

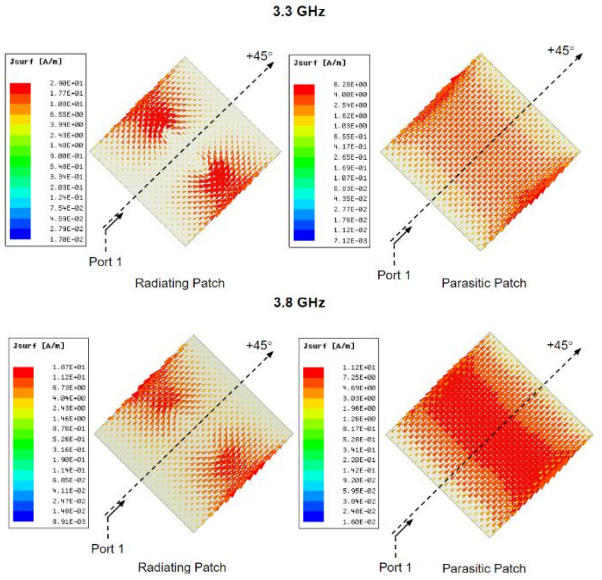


Fig. 2. Surface currents on the main and parasitic patches.

## III. NUMERICAL STUDIES

### A. Parametric analyses

Proposed SPA is modeled and simulated in Ansoft HFSS. Its electrical performances are numerically analyzed in terms of impedance matching ($|S_{11}|$) and port isolation ($|S_{21}|$) with parametric studies. Each parametric study is carried out by sweeping one parameter within a range while the rest is kept fixed. Since SPA ports are built in symmetric configuration, only $|S_{11}|$ results at port 1 are reported. Upper and lower boundaries of the desired band

of operation (3.30-3.80 GHz) are shown with vertical black dashed lines in the figures.

$|S_{11}|$ and $|S_{21}|$ characteristics of SPA as a function of main patch height ($h_{s1}$) are given in Fig. 3. In this analysis, $h_{s1}$ is swept in 1-3 mm range by 1 mm steps. Proposed SPA reaches its best matching level and largest impedance BW when $h_{s1}$ is set to 2 mm. In addition, typical port isolation is obtained to be $|S_{21}| < -26$ dB at this value of $h_{s1}$.

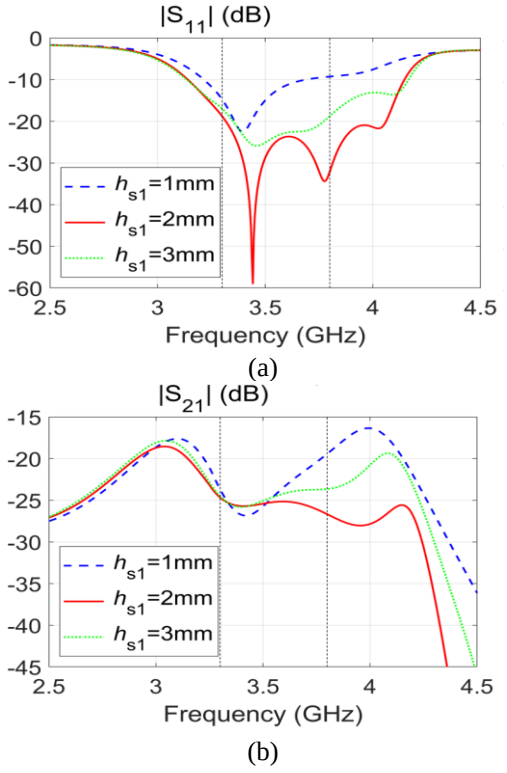


Fig. 3. Effect of the main patch height on (a) $|S_{11}|$ and (b) $|S_{21}|$.

The same procedure is also carried out for the parasitic patch height ($h_{s2}$) and the best performance is achieved when $h_{s2} = 7$ mm as shown in Fig. 4. With these values ($h_{s1} = 2$ mm, $h_{s2} = 7$ mm), effect of parasitic patch can be seen better in Fig. 5 (a) showing that desired matching level and impedance BW cannot be achieved by a single patch. Figure 5 (b) plots the simulations of radiation pattern of SPA in azimuth plane ($\theta = 90°$, $-180° < \phi < 180°$) by changing $h_{s1}$ with fixed $h_{s2} = 7$ mm. It is observed that FBR gets better at lower $h_{s1}$ values. As a result, the basic idea of this design to place main patch at the lowest possible height to have good FBR and utilize parasitic one to reach desired matching level, impedance BW and isolation is consistent. Moreover, Fig. 5 (b) shows that higher FBR can be attained without using any reflector by only positioning the main patch at lower heights.

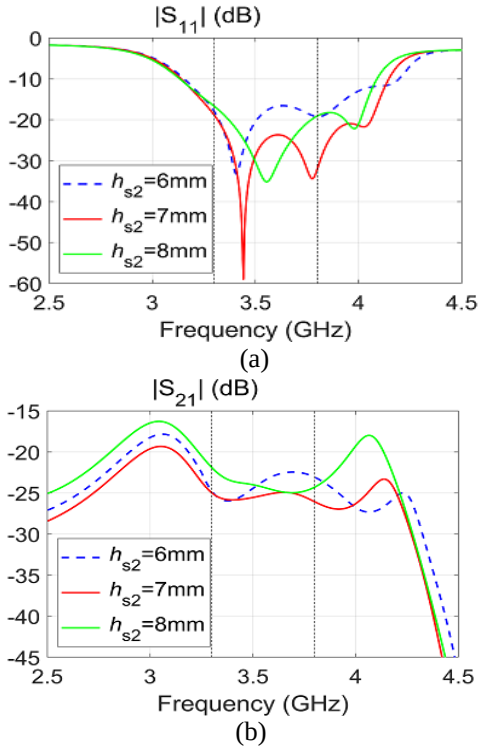


Fig. 4. Effect of the parasitic patch height on (a) $|S_{11}|$ and (b) $|S_{21}|$.

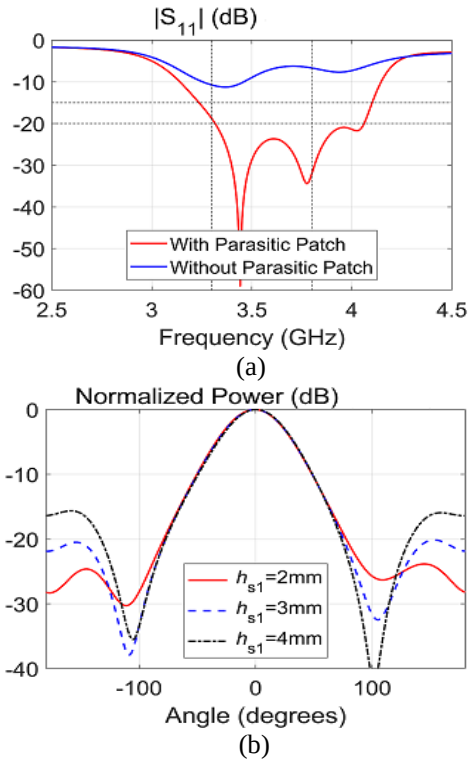


Fig. 5. $|S_{11}|$ and FBR graphs (a) effect of the parasitic patch on $|S_{11}|$, and (b) effect of $h_{s1}$ on FBR.

Figure 6 illustrates $|S_{11}|$ and $|S_{21}|$ performance of SPA regarding axial ratio ($A_x$) of the elliptic-H slots. This analysis is carried out as $A_x$ is increased from 14.5 to 18.5 with increment of 1. When $A_x$ = 16.5, antenna has two resonance points at 3.39 GHz and 3.74 GHz and 20% impedance BW for $|S_{11}| < -15$ dB. Port isolation does not vary much with respect to $A_x$ in desired band. $|S_{21}|$ is typicallly < –26 dB.

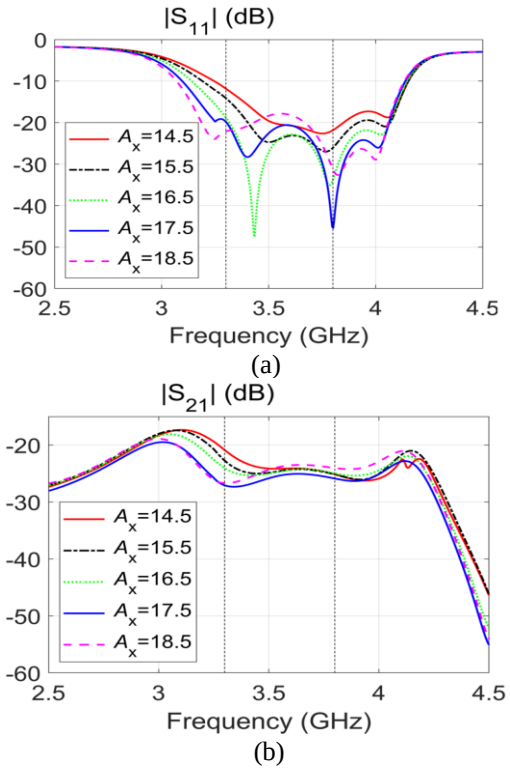


Fig. 6. Effect of $A_x$ of elliptic slot on (a) $|S_{11}|$ and (b) $|S_{21}|$.

### B. Effect of elliptic H-slots

Effect of the elliptic-H slots on the SPA performance is evaluated by comparing it with rectangular-H slots having the same length ($L_s$ = 15.98 mm) and area ($A_s \approx$ 11.186 mm$^2$). Results are illustrated in Fig. 7 and Fig. 8. Elliptic-H slots improve matching level appreciably in the desired band. Port isolation is also improved by elliptic-H slots approximately 2.5 dB with respect to rectangular-H slots. For better understanding, comparison of the port isolation mechanism is also demonstrated with the currents flowing on the slot plane of feed line layer at 3.55 GHz. As shown in Fig. 8, the current distribution on the elliptic-H slots, aspecially around the center where most mutual coupling occurs between ports, are weaker than that of the rectangular-H slots. This weaker flowing current results in improvement in the port isolation.

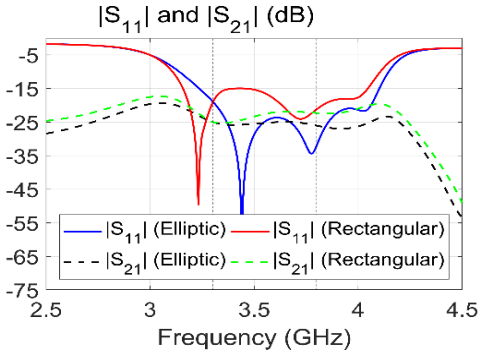


Fig. 7. Comparison of elliptic-H and rectangular-H slots.

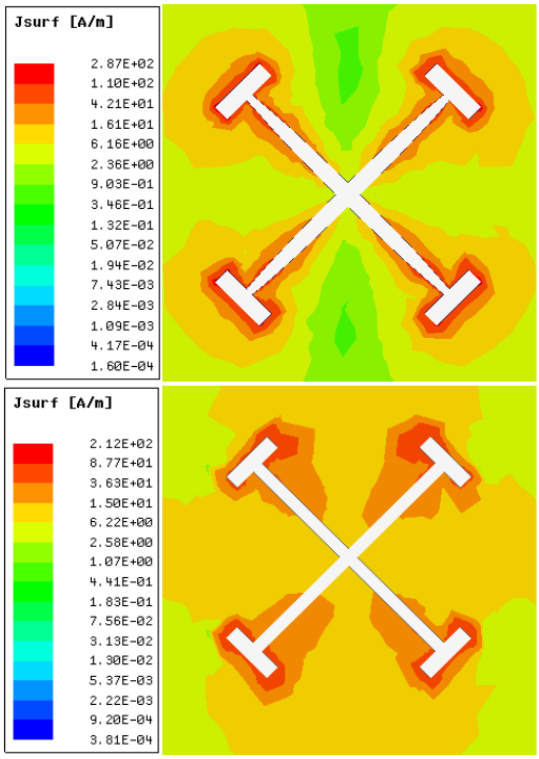


Fig. 8. Current distributions on the slot plane with elliptic-H and rectangular-H slots.

## IV. MEASUREMENT RESULTS

Proposed SPA is prototyped in accordance with design descriptions given in Section II and is shown in Fig. 9. Air layers are formed by using plastic separators with appropriate heights. Overall size of the prototype SPA is 110 × 110 × 11.1 mm$^3$. Numerical results of Section III are experimentally verified by the measurements of S-parameters ($|S_{11}|$, $|S_{22}|$, and $|S_{21}|$) and radiation patterns (co-pol, cross-pol). S-parameters are measured by HP 8720D vector network analyzer and radiation pattern measurements are performed in an anechoic chamber.

Measurements are taken when the SPA is excited at port 1 (+45º polarization) while the other port is terminated by broadband 50 Ω load. Again due to the symmetric configuration of ports, results of port 2 (−45º polarization) are not included.

(a) (b) (c)

Fig. 9. Prototyped SPA (a) feed network, (b) elliptic-H slots, and (c) top view (not in scale).

Figure 10 plots measured and simulated S-parameters of SPA. It can be seen that measured results are consistent with the simulations. SPA exhibits 22.1% impedance BW for $|S_{11}|$, $|S_{22}| < -15$ dB along 3.14-3.92 GHz. Slight discrepancy between $|S_{11}|$ and $|S_{22}|$ is caused by the air bridge. The measured $|S_{21}|$ is < −28 dB in desired band of 3.30-3.80 GHz.

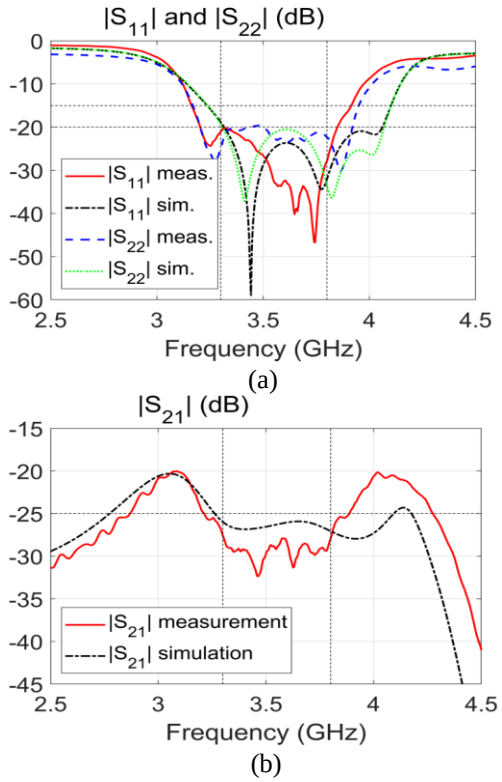


Fig. 10. Measured and simulated S-parameters (a) $|S_{11}|$, $|S_{22}|$, and (b) $|S_{21}|$.

Normalized co/cross-pol radiation patterns in elevation and azimuth planes are measured at 3.30 GHz, 3.55 GHz, 3.80 GHz frequencies within the operating band. Both simulations and measurement results, which are consistent with each other, are plotted in Fig. 11. SPA exhibits stable, symmetric and directional radiation patterns in both planes. Measured HPBWs are 65°, 62° and 57° in elevation plane and 64º, 62º and 60º in azimuth plane at the corresponding frequencies, respectively. Gain of the SPA in the operating band varies between 8.6-9.1 dBi and given in Fig. 12. High FBR, one of the design goals, is achieved to be > 27 dB. From Fig. 11, it is observed that cross-polar discrimination (XPD) level, which is another important performance criterion of base station antenna and not targeted in this study, is also very good. That is, XPD level at boresight is > 25 dB.

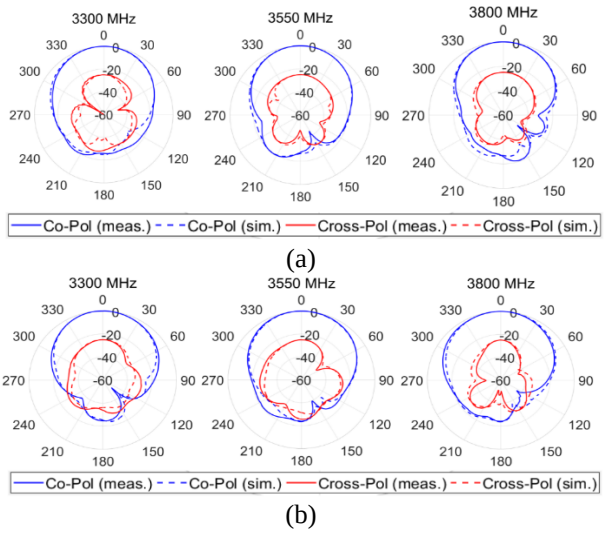


Fig. 11. Measured and simulated co-/cross-pol patterns in (a) elevation plane and (b) azimuth plane.

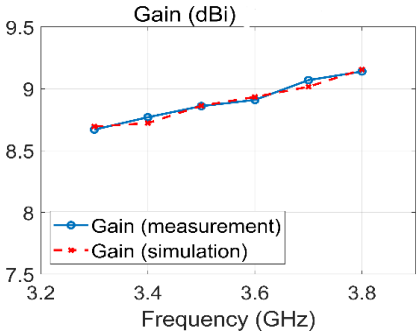


Fig. 12. Measured and simulated gain of the SPA.

## V. CONCLUSION

In this paper, compact, dual-polarized, broadband,

slot-coupled SPA with ease of fabrication is designed and investigated for Sub-6 GHz 5G base station applications. Proposed SPA is made up of main patch and parasitic patch layers above feedline layer and is excited by crossed elliptic-H slots creating ±45° dual slant polarizations. To summarize, proposed SPA exhibits 22.1% (3.14-3.92 GHz) impedance BW for $|S_{11}|$, $|S_{22}| < -15$ dB, port isolation $|S_{21}| < -28$ dB and FBR > 27 dB. It has HPBWs of 57°-65° and 60°-64° in elevation and azimuth planes, respectively with varying gain of 8.6-9.1 dBi.

Simulated and measured radiation patterns show that proposed SPA is low profile with high isolation and high FBR. In this design, placement of the main patch at a reasonably low height, then use of parasitic patch in combination with it and use of elliptic-H slots, all together provides the solution and helps to reach design goals for impedance BW, matching level, isolation and FBR with no reflector plane, cavity-backed structure, EBG or meta-material based surface. Moreover, overall height of the proposed antenna is still low profile (11.1 mm) as it can be verified among similar works in Table 2. Table 2 lists the performances of proposed work and some similar existing ones designed to operate in the same band (3.30-3.80 GHz) as a base station antenna. To make full comparison, note that [3-5] are patch antennas with probe feeding while [12-16] are patch antennas with slot coupling. As can be seen from Table 2, proposed SPA outperforms all of the slot coupled antennas [12-16] and competes with the probe-fed antennas [3-4] by satisfying all the desired performance parameters of base station antennas. Considering the numerical and experimental results, proposed SPA can be a good candidate to be used in and to facilitate the mMIMO array design for 5G applications.

## ACKNOWLEDGMENT

The authors would like to acknowledge the support of The Scientific and Technological Research Council of Turkey (TUBITAK) under Grant No. 3180114.

Table 2: Comparison of proposed antenna with the related previous works

| Work | BW (GHz, %) | $\|S_{11}\|$, $\|S_{22}\|$ (dB) | $\|S_{21}\|$ (dB) | FBR (dB) | Height (mm) | Reflector |
|---|---|---|---|---|---|---|
| [3] | 3.15-4.55, 37% | < –10 dB | < –38 | > 12.5 | 12.7 | N/A |
| [4] | 2.86-4.12, 36% | < –15 dB | < –30 | > 28 | 13.4 | N/A |
| [5] | 3.13-4.16, 28.3% | < –15 dB | < –23 | > 10 | 29.2 | N/A |
| [12] | 3.30-3.80, 14% | < –10 dB | < –20 | > 30 | 37.2 | W |
| [13] | 3.33-3.83, 14% | < –10 dB | < –23 | > 25 | 34 | W |
| [14] | 3.23-3.80, 17% | < –10 dB | < –50 | > 10 | 10.5 | W/O |
| [15] | 3.25-3.80, 15.6% | < –15 dB | < –25 | > 18 | 12.2 | W |
| [16] | 3.30-3.60, 8.9% | < –15 dB | < –25 | > 16 | 18.8 | W |
| This work | 3.10-3.99, 25.1%, 3.14-3.92, 22.1% | < –10 dB < –15 dB | < –28 | > 27 | 11.1 | W/O |

W: With reflector, W/O: Without reflector, N/A: Not applicable.

## REFERENCES

[1] P. K. Mishra, D. R. Jahagirda, and G. Kumar, "A review of broadband dual linearly polarized microstrip antenna designs with high isolation," *IEEE Antennas Propag. Mag.*, vol. 56, no. 6, pp. 238-251, Dec. 2014.

[2] H-W. Lai and K-M. Luk, "Dual polarized patch antenna fed by meandering probes," *IEEE Trans. Antennas Propag.*, vol. 55, no. 9, pp. 2625-2627, Sept. 2007.

[3] K. S. Ryu and A. A. Kishk, "Wideband dual-polarized microstrip patch excited by hook shaped probes," *IEEE Trans. Antennas Propag.*, vol. 56, no. 12, pp. 3645-3649, Dec. 2008.

[4] M. Ciydem and A. E. Miran, "Dual polarization wideband sub-6 GHz suspended patch antenna for 5G base stations," *IEEE Antennas Wirel. Propag. Lett.*, vol.19, no. 7, pp. 1142-1146, July 2020.

[5] P. Chen, L. Whang, and T. Ding, "A broadband dual-polarized antenna with CRR-EBG structure for 5G applications," *Applied Computational Electromagnetics Society Journal*, vol. 35, no. 21, pp. 1507-1512, Dec. 2020.

[6] J.-J. Xie, Y.-Z. Yin, J.-H. Wang, and X.-L. Liu, "Wideband dual-polarized electromagnetic fed patch antenna with high isolation and low cross-polarization," *IET Electron. Lett.*, vol. 49, no. 3, pp. 171-173, Jan. 2013.

[7] Y. Jin and Z. Du, "Broadband dual-polarized F-probe fed stacked patch antenna for base stations," *IEEE Antennas Wirel. Propag. Lett.*, vol. 14, pp. 1121-1124, Jan. 2015.

[8] K. M. Mak, H. W. Lai, and K. M. Luk, "A 5G wideband patch antenna with antisymmetric

L-shaped probe feeds," *IEEE Trans. Antennas Propag.*, vol. 66, no. 2, pp. 957-961, Feb. 2018.

[9] M. Barba, "A high-isolation, wideband and dual-linear polarization patch antenna," *IEEE Trans. Antennas Propag.*, vol. 56, no. 5, pp. 1472-1476, May 2008.

[10] A. A. Serra, P. Nepa, G. Manara, G. Tribellini, and S. Cioci, "A wideband dual-polarized stacked patch antenna," *IEEE Antennas Wirel. Propag. Lett.*, vol. 6, pp. 141-143, Apr. 2007.

[11] K.-L. Wong, H.-C. Tung, and T.-W. Chiou, "Broadband dual-polarized aperture-coupled patch antennas with modified H-shaped coupling slots," *IEEE Trans. Antennas Propag.*, vol. 50, no. 2, pp. 188-191, Aug. 2002.

[12] R. Caso, A. Serra, A. Buffi, M. R-Pino, P. Nepa, and G. Manara, "Dual-polarized slot-coupled patch antenna excited by a square ring slot," *IET Microw. Antennas Propag.*, vol. 5, no. 5, pp. 605-610, Apr. 2011.

[13] C. Hua, R. Li, Y. Wang, and Y. Lu, "Dual-polarized filtering antenna with printed Jerusalem-cross radiator," *IEEE Access*, vol. 6, pp. 9000-9005, Feb. 2018.

[14] J. Lu, Z. Kuai, X. Zhu, and N. Zhang, "A high-isolation dual-polarization microstrip patch antenna with quasi-cross-shaped coupling slot," *IEEE Trans. Antennas Propag.*, vol. 59, no. 7, pp. 2713-2717, 2011.

[15] A. Alieldin, Y. Huang, M. Stanley, S. D. Joseph, and D. Lei, "A 5G MIMO antenna for broadcast and traffic communication topologies based on pseudo inverse synthesis," *IEEE Access*, vol. 6, pp. 65935-65945, Oct. 2018.

[16] H. Huang, X. Li, and Y. Liu, "5G MIMO antenna based on vector synthetic mechanism," *IEEE Antennas Wirel. Propag. Lett.*, vol. 17, no. 16, pp. 1052-1055, June 2018.

[17] J. Jiang, Y. Li, L. Zhao, and X. Liu, "Wideband MIMO directional antenna array with a simple meta-material decoupling structure for X-band applications," *Applied Computational Electromagnetics Society Journal*, vol. 35, no. 5, pp. 556-566, May 2020.

[18] F. Liu, J. Guo, L. Zhao, G-L. Huang, Y. Li, and Y. Yin, "Dual-band metasurface-based decoupling method for two closely packed dual-band antennas," *IEEE Trans. Antennas Propag.*, vol. 68, no. 1, pp. 552-557, Jan. 2020.

[19] A. M. Abbosh, "Ultra-wideband vertical microstrip - microstrip transition," *IET Microw. Antennas Propag.*, vol. 1, no. 5, pp. 968-972, Oct. 2007.

**Mehmet Ciydem** was born in 1971 in Ankara, Turkey. He received his B.Sc., M.Sc. and Ph.D. degrees all in Electrical Engineering from Middle East Technical University (METU), Ankara, Turkey with high honors. After working in defense industry (Aselsan, Havelsan, TAI) for many years, he founded Engitek Ltd. company in 2009, where he is President. He is an Associate Professor of Electromagnetic Theory and Communications lecturing occasionally in several universities (Bilkent Univ., Gazi Univ., Karatay Univ., Hacettepe Univ., and Army War Academy). His research interests are in the areas of electromagnetics, wave propagation, antennas, RF/ microwave engineering, radar and communication systems.